PROCEEDINGS OF THE ROYAL SOCIETY A

CrossMark click for updates

Proc. R. Soc. A (2012) **468**, 3533–3551
doi:10.1098/rspa.2012.0008
Published online 25 July 2012

Modelling the mechanical response of *urushi* lacquer subject to a change in relative humidity

BY X. LIU[1,*], R. D. WILDMAN[2], I. A. ASHCROFT[2], A. E. ELMAHDY[1] AND P. D. RUIZ[1]

[1] *School of Mechanical and Manufacturing Engineering, Loughborough University, Loughborough LE11 3TU, UK*
[2] *Faculty of Engineering, University of Nottingham, University Park, Nottingham, NG7 2RD, UK*

A hygromechanical model has been developed to simulate the in-service behaviour of the natural lacquer *urushi*, using a phenomenological description of viscoelasticity. The material and mechanical properties were determined as a function of the relative humidity (RH), and the relationship between RH and moisture content was determined. These properties served as inputs to a finite-element-based model that was then tested against experimental measurements of the depth-averaged stresses in a thin layer of *urushi* deposited on a substrate and exposed to changes in the environmental conditions. Good agreement was seen between the predicted and measured behaviour. The validated model was used to investigate the spatial and temperature variation of stress in *urushi* films subjected to cyclic environmental conditioning.

Keywords: viscoelasticity; modelling; *urushi*

1. Introduction

Urushi is a complex natural polymeric material obtained from the sap of the tree, *Rhus verniciflua*, which, when cured, provides a hard, durable and aesthetically pleasing coating for delicate objects (Taguchi *et al.* 2007). These properties have led to the use of *urushi* in the coating of furniture and small decorative items in East Asia for hundreds of years (McSharry *et al.* 2007). However, exposure to environmental conditions such as varying humidity and temperature and long-term exposure to ultraviolet (UV) radiation leads to ageing-related damage (Liu *et al.* 2010, 2011). An example of this was seen on the object known as the Mazarin Chest, which showed distinct signs of lacquer damage before its recent restoration (Bratasz *et al.* 2008). When considering the conservation of such an object, questions arise regarding the suitability of treatments, and surprisingly, there has been little scientific exploration of this up to now. A need arises, therefore, to explore the material properties, the environmental conditions, their interaction and the consequences for the conservation of important cultural objects.

*Author for correspondence (x.p.liu@sheffield.ac.uk).

Received 4 January 2012
Accepted 26 June 2012

A number of studies of *urushi* have shown that it is largely viscoelastic (Ogawa *et al.* 1998*a*) and have demonstrated some of the effects of both humidity and UV exposure on its behaviour (Ogawa *et al.* 1998*a*; Obataya *et al.* 2002). One study observed the effect of high relative humidity (RH) on delamination (Ogawa *et al.* 1998*a*), and Obataya *et al.* (2001) showed that moisture content significantly affects the viscoelastic properties of *urushi*. Ogawa *et al.* (1998*b*) investigated the effect of exposing East Asian lacquer films to UV and showed that hardness and elastic modulus increased with exposure time, whereas the tensile strength and the elongation at break decreased. They proposed that the increased hardness was related to a cross-linking reaction involving the enzyme laccase. Rivers (2003) explored the effect of exposure to UV radiation on the surface appearance of *urushi* and noted how the lacquer fades and becomes dull as light breaks down the molecular structure.

Recently, Elmahdy *et al.* (2011) were able to measure the stresses in a thin layer of *urushi* as it responded to changes in moisture. They considered the behaviour of a layer of *urushi* deposited onto a small disc, which was then placed within a chamber with controlled temperature and humidity. This sample was then subjected to a rapid change in environmental humidity and the curvature induced in the sample measured and related to the stress developed in the *urushi* layer. The measurements were conducted using phase-shifting interferometry, a powerful technique for measuring small whole-field displacements developed in a range of complex materials, such as composites (Ruiz *et al.* 2006), biological (Yang *et al.* 2007), foodstuffs (Saleem *et al.* 2003, 2005) and polymers (Morita *et al.* 2008). In this case, Elmahdy *et al.* (2011) measured the out-of-plane displacements, and through an extension of Stoney's equation (Stoney 1909; Atkinson 1997), observed the evolution of stresses as moisture was removed. This experiment presents an ideal system for validating any proposed model, because the observed behaviour will depend upon the precise details of the constitutive relationships for hygroscopic transport, the rheological model and their coupling.

Modelling of the observed *urushi* behaviour has been limited to date. Ogawa & Kamei (2000) used the finite element method to explore the effect of moisture on fracture, but limited themselves to an assumption of elastic material properties. However, it has been conclusively demonstrated that viscoelasticity in *urushi* is not only non-negligible, but that the viscoelastic response is also strongly influenced by both moisture content and ageing (Bratasz *et al.* 2008; Liu *et al.* 2010, 2011; Elmahdy *et al.* 2011). This study aims to address this lack of a validated viscoelastic model and its coupling to the ingress and transport of moisture in *urushi*. Section 2 of this study will introduce the proposed model, §3 will discuss the experimental methodology required to identify the relevant constitutive relationships, their form and values. In §4, a solution methodology for the model will be obtained, and then in §5, this will be validated against the results of Elmahdy *et al.* (2011) and the internal mechanics discussed.

2. A model for a thin layer of *urushi*

When used for protective purposes, a thin layer of *urushi* lacquer is cured on the surface of a substrate, usually wood. The resultant stresses developed in the *urushi* are a result of competition between response to environmental changes

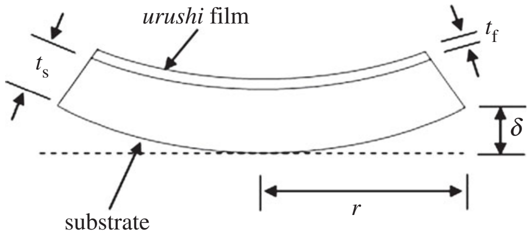

Figure 1. Deflection of an initially flat substrate owing to film shrinkage.

(e.g. thermal expansion, hygroscopic expansion or volume and material property changes owing to ageing) and the constraint of the substrate (which itself might deform in some manner), as shown in figure 1. In equilibrium, the spatial variation of stresses in a thin layer can be approximated as

$$\frac{\partial \sigma_x}{\partial x} + \frac{\partial \sigma_{xy}}{\partial y} = 0 \tag{2.1}$$

and

$$\frac{\partial \sigma_y}{\partial y} + \frac{\partial \sigma_{xy}}{\partial x} = 0, \tag{2.2}$$

where σ_x and σ_y are normal stress components in the x and y directions, respectively, and σ_{xy} is the shear stress.

In order to solve these equations, constitutive relations that relate the strain to stress must be prescribed. These can be quite general, and in the case of polymeric materials, are often time-dependent, such that the stress is given by

$$\sigma = f\left(\varepsilon, \frac{\mathrm{d}\varepsilon}{\mathrm{d}t}\right), \tag{2.3}$$

where the exact functional relationship needs to be determined. Polymeric materials are usually able to absorb moisture, and will change dimensions accordingly. In this case, the hygroscopic strain developed as a function of this moisture ingress is given by

$$\varepsilon_{\mathrm{h}} = \beta C, \tag{2.4}$$

where $\varepsilon_{\mathrm{h}}, \beta$ and C are the hygroscopic strain, coefficient of hygroscopic strain and moisture concentration, respectively, where β needs to be determined experimentally. Finally, boundary conditions that constrain the system need to be specified and these are problem-specific.

Because the moisture can directly affect the strain in the material, a stress analysis will need to be coupled with a model of the moisture absorption and diffusion. In general, diffusion is described by a combination of a continuity equation

$$\frac{\partial \varphi}{\partial t} + \nabla \cdot f = 0, \tag{2.5}$$

where φ, f and t are density of diffusing material, flux and time, respectively, and a diffusive constitutive law,

$$\frac{\partial \varphi}{\partial t} = \nabla \cdot [D \cdot \nabla \varphi], \tag{2.6}$$

where D is diffusion coefficient.

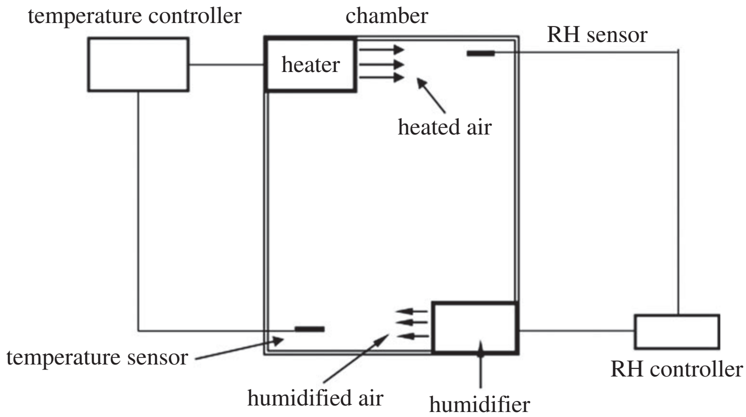

Figure 2. Schematic of the controlled environment chamber used to cure *urushi* thin films and to maintain a constant environment during testing.

It can be seen, therefore, that in order to develop a model for the development of stresses in *urushi* that are a consequence of environmental changes, a hygro-mechanical definition of material is required.

3. Material properties

(a) Identification of the material rheology

In order to characterize the behaviour of *urushi*, a procedure for producing films in a controlled manner was developed, enabling reproduction and testing of their mechanical, hygroscopic and absorption behaviour. The first step was to filter any impurities from the liquid *urushi*. *Kijiro urushi* (Wantanabe Syoten Co., Japan) was squeezed through rayon paper in a replication of a traditional Japanese filtering technique (Rivers 2003). This was repeated seven times. The material was then deposited onto a substrate of the required size and allowed to cure at $75 \pm 1\%$ RH and $23 \pm 2°$C.

A series of mechanical tests was conducted to identify the characteristic rheological properties, including constant displacement rate tests and creep and recovery tests at different RHs. Film samples were prepared using the methodology described earlier and cut into rectangular strips of 60×5 mm in size. The thickness of each strip was measured using a Mitutoyo digital micrometer, accurate to 1 µm and found to be in a range between 60 and 100 µm. The humidity was monitored and either increased or decreased using a controller connected to a combination of a wet, blown air system and a dessicant to absorb excess moisture (figure 2). The temperature was maintained at 23°C using a heating element. The mechanical tests were performed using an Instron universal testing machine 5569 with a 100 N load cell at RHs of 30, 50 and 75 per cent. Prior to each test, the films were kept for one week under constant RH (30, 50 and 75%) to ensure that equilibrium had been reached (Liu *et al.* 2011, 2012).

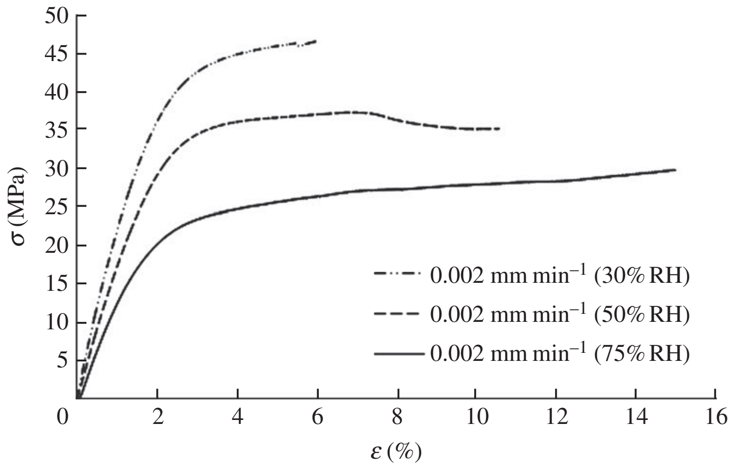

Figure 3. Stress–strain curves from tensile tests performed at $0.002\,\mathrm{mm\,min^{-1}}$ on *urushi* film samples after saturation at different relative humidities (shown in legend).

Table 1. Tensile elastic modulus (E), tensile strength at break (σ_B) and strain at break (ε_B) for *urushi* film samples after saturation at different relative humidities (RHs) from constant displacement rate tests at $0.002\,\mathrm{mm\,min^{-1}}$.

RH (%)	E (MPa)	σ_B (MPa)	ε_B (%)
30	2298.2	46.6	5.8
50	1736.4	35.2	10.4
75	1356.8	29.7	14.8

Uniaxial loading at a constant displacement rate ($0.002\,\mathrm{mm\,min^{-1}}$) was performed for *urushi* samples saturated under different RHs to obtain estimates of the tensile strength, elastic modulus and fracture strain (table 1). The stress–strain plots in figure 3 show that as the humidity is increased, the elastic region and modulus reduce and the fracture strain increases, which is consistent with the ingressed moisture acting as a plasticizer (Zhang *et al.* 2002). Creep and recovery tests were performed at a range of humidities and constant stresses (30, 50, 60 and 70% of their tensile strength at break) by applying a constant load and recording the subsequent deformation as a function of time. After 12 h, the load was removed and a 12 h recovery observed. Figure 4*a*–*c* shows the observed behaviour for different humidities. This behaviour is typical for a viscoelastic response: a rapid increase in strain, followed by a reduction in strain rate to a constant, but non-zero value and an instantaneous recovery followed by a relaxation to an asymptotic, non-zero strain.

A previous analysis of *urushi* showed that it can be modelled using a modified generalized Kelvin fluid (MGKF) model composed of nonlinear Maxwell and multiple Kelvin units connected in series, as shown in figure 5 (Liu *et al.* 2011).

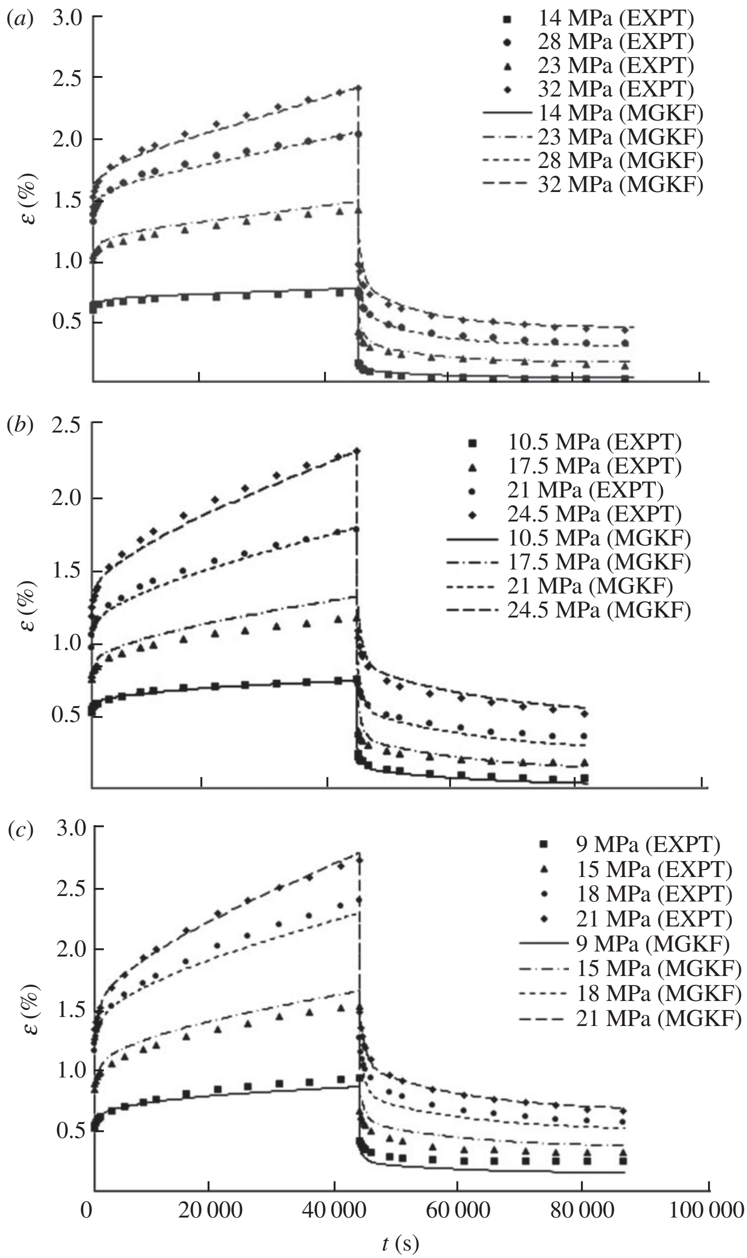

Figure 4. (*a*) Experimental (EXPT) and predicted (MGKF) creep and recovery data for *urushi* film samples saturated under 30% RH at a range of constant engineering stresses (shown in the legend). (*b*) Experimental (EXPT) and predicted (MGKF) creep and recovery data for *urushi* film samples saturated under 50% RH at a range of constant engineering stresses (shown in the legend). (*c*) Experimental (EXPT) and predicted (MGKF) creep and recovery data for *urushi* film samples saturated under 75% RH at a range of constant engineering stresses (shown in the legend).

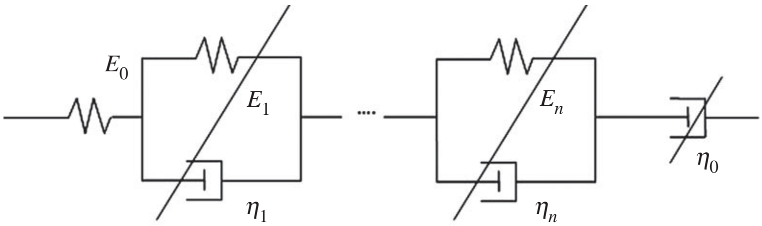

Figure 5. A modification of Burgers model to form a generalized Kelvin fluid model (Liu *et al.* 2011), where the slash indicates nonlinearity.

Table 2. Parameters derived from a modified generalized Kelvin fluid creep and recovery model for fresh *urushi* film.

RH (%)	test	E_0 (%)	μ	λ	τ_1 (s)	m	n	τ_2 (s)
30	creep	2256 ± 4.7	8947.0	4157.3	500.0	2.71	1.28	9876.5
	recovery		5303.0	490.88	724.4	3.15	2.05	10081.6
50	creep	2177 ± 6.5	8009.9	3400.1	531.9	2.70	1.25	10000.3
	recovery		776.52	1746.6	835.3	4.63	1.29	20394.7
75	creep	1711 ± 6.1	8488.5	3487.1	819.8	2.56	1.13	10204.1
	recovery		117 471	567.07	905.6	1.82	1.67	16934.9

It was shown that this was able to capture reasonably well all the components of the creep behaviour of *urushi*. Mathematically, the uniaxial behaviour for the creep and recovery strains (ε_c and ε_r) are given by (Liu *et al.* 2011):

$$\varepsilon_c(t) = \frac{\sigma_c}{E_0} + \left(\frac{\sigma_c}{\mu}\right)^m t + \sum_{i=1}^{N}\left(\frac{\sigma_c}{\lambda}\right)^n \left(1 - \exp\left(\frac{-t}{\tau_i}\right)\right), \quad (t_0 \le t < t_1) \tag{3.1}$$

and

$$\varepsilon_r(t) = \frac{\sigma_r}{E_0} + \left(\frac{\sigma_0}{\mu}\right)^m t_1 + \sum_{i=1}^{N}\left(\frac{\sigma_0}{\lambda}\right)^n \left(\exp\left(\frac{t_1}{\tau_i}\right) - 1\right) \exp\left(\frac{-t}{\tau_i}\right), \quad (t \ge t_1), \tag{3.2}$$

where t_0 is the time when the load is applied, t_1 is the time when the load is removed, μ, λ, $\tau_i (i \ge 1)$, m and n are rheological parameters and σ_c and σ_r are the stresses during creep and recovery, respectively. Parameter σ_0 is the magnitude of the reduction of the applied stress, and is equal to the difference between σ_c and σ_r. These parameters were determined employing a nonlinear regression analysis using Matlab (Lagarias *et al.* 1998). A number of values of N were used in equations (3.1) and (3.2), but no significant improvement in fitting to the data was obtained for $N > 2$. The rheological parameters for each humidity are shown in table 2. Because the behaviour for each term in equations (3.1) and (3.2) is controlled by more than one parameter, interpretation is difficult.

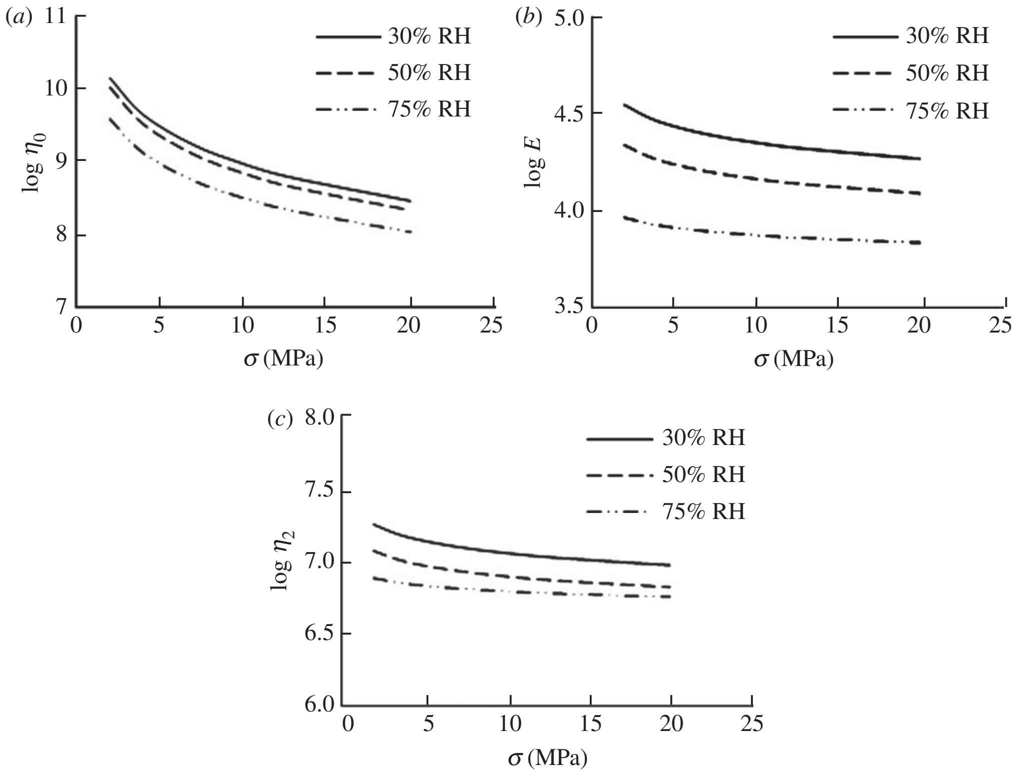

Figure 6. (*a*) Effect of RH on the viscoelastic coefficients of the modified generalized Kelvin fluid model for *urushi* films (equation (3.3)) at different RH (shown in legend). (*b*) Effect of RH on the viscoelastic coefficients of the modified generalized Kelvin fluid model for *urushi* films (equation (3.4)) at different RH (shown in legend). (*c*) Effect of RH on the viscoelastic coefficients of the modified generalized Kelvin fluid model for *urushi* films (equation (3.5)) at different RH (shown in legend).

To facilitate characterization, these parameters were translated into apparent quantities similar to the more familiar Newtonian viscous and Hookian elastic coefficients, such that

$$\eta_0 \equiv \frac{\mu^m}{\sigma^{m-1}}, \tag{3.3}$$

$$E \equiv \frac{\lambda^n}{\sigma^{n-1}} \tag{3.4}$$

and

$$\eta_i \equiv \frac{\tau_i \lambda^n}{\sigma^{n-1}}. \tag{3.5}$$

These apparent quantities are plotted as a function of stress in figure 6. This shows that firstly, the magnitude of all the parameters decreases as the stress is increased. Secondly, in each case, the magnitude decreases as the RH increases, indicating that as moisture is absorbed, there is a tendency for the resistance to deformation to reduce.

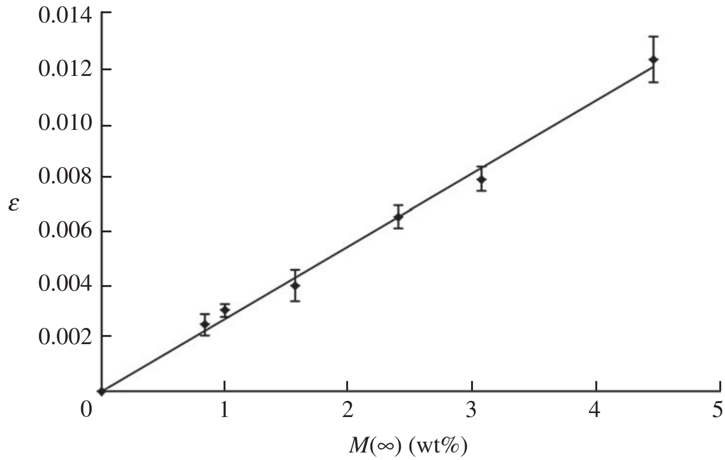

Figure 7. The measured hygroscopic strain of saturated samples as a function of moisture content, with error bars showing s.d.

Table 3. Relative humidities maintained by different salt solutions on saturation inside a sealed container.

$MgCl_2$	K_2CO_3	NaBr	NaCl	KCl	K_2S
$33.8 \pm 0.8\%$	$43.2 \pm 0.6\%$	$58.6 \pm 1.2\%$	$75.0 \pm 0.9\%$	$85.0 \pm 1.2\%$	$95 \pm 1.8\%$

(*b*) *Coefficient of hygroscopic expansion*

To obtain the coefficient of hygroscopic expansion, β, the filtered *urushi* material was deposited onto 120×75 mm rectangular glass substrates using a spin coater calibrated to achieve samples of thickness of 0.06–0.08 mm (Elmahdy *et al.* 2011). These films were then left to cure at a temperature of $23 \pm 2°$C and RH of $75 \pm 1\%$ for three weeks. After curing, the films were removed from the glass substrate and cut into rectangular strips with lateral dimensions of 120×10 mm. These were then stored in a desiccator until the weight change was less than 0.1 per cent per week. The dry samples were marked and photographed, after which they were placed into sealed containers with a range of RHs, controlled by the salt solutions presented in table 3. Once saturation had been achieved, the sample was photographed once again, and the change in the sample dimensions measured. This was repeated for a number of RHs to identify any variance in β with moisture content. Figure 7 shows that there is an approximately linear relationship between hygroscopic strain and moisture content, including a moisture-content-independent coefficient of hygroscopic expansion, which, in this case, was 0.0027 $(\text{wt}\%)^{-1}$.

(*c*) *Diffusion*

The rate of moisture absorption was characterized by gravimetric tests in which the mass of a sample was monitored as a function of time following a change in RH. A digital balance HA180 (A&D Instruments Ltd) with a precision of

0.1 mg was used for all the weight measurements. Three samples of dimensions 70×50 mm were prepared. Each of the samples has a uniform thickness of 0.06–0.08 mm. Samples were allowed to reach a uniform moisture distribution by storing them in a curing chamber at 30 per cent RH, until there was no change in the mass of the sample. After that, the samples' environment was changed to 40, 50 and then to 60 per cent RH, where each humidity was maintained for 16 h and the samples' mass was observed every 30 min. Finally, the samples were dried at 100°C for 27 h to remove the moisture, and the dry weight obtained. The time-dependent moisture content, $M(t)$, is given by

$$M(t) = \frac{m_t - m_{\mathrm{dry}}}{m_{\mathrm{dry}}} \times 100, \tag{3.6}$$

where m_t is the mass of the specimen at time t, and m_{dry} is the mass of the dry specimen.

The plotted points in figure 8 show the moisture content as a function of time for *urushi* film for various changes of RH. The main features are that the moisture gain increases with RH and that the curves appear to show Fickian diffusion (Crank 1975). This suggests that an analysis of the data can be performed to extract the diffusion coefficient, D, using the equations of Fickian diffusive transport. Therefore, combining equation (2.5) with Fick's first law of diffusion in one dimension

$$F = -D\frac{\partial C}{\partial x}, \tag{3.7}$$

where F is the mass flux of moisture, C is the concentration of moisture, x is the space coordinate measured normal to the section and D is a spatially and concentration-independent diffusion coefficient, leading to Fick's Second Law

$$\frac{\partial C}{\partial t} = D\frac{\partial^2 C}{\partial x^2}. \tag{3.8}$$

For a case of a semi-infinite plane sheet diffusion problem with a thickness of t_f, the initial condition can be defined as

$$C(x, 0) = C_0, \quad \text{at} \quad t = 0 \quad \text{and} \quad 0 \leq x \leq t_f, \tag{3.9}$$

where C_0 is the initial concentration.

If the sheet is exposed to an environment with a different moisture concentration, the boundary conditions are

$$C(x, t) = C_{\mathrm{s}} \quad \text{at} \quad x = 0 \quad \text{and} \quad x = t_f \quad \text{at} \quad t > 0, \tag{3.10}$$

where C_{s} is the surface moisture concentration corresponding to the environmental RH.

The solution of equation (3.8) for this case is well known (Crank 1975):

$$C(x, t) = C_{\mathrm{s}} + \sum_{j=0}^{\infty} \frac{4(C_0 - C_{\mathrm{s}})}{\pi(2j+1)} \sin\left(\frac{(2j+1)\pi x}{t_f}\right) \exp\left(-\left(\frac{(2j+1)\pi}{t_f}\right)^2 Dt\right). \tag{3.11}$$

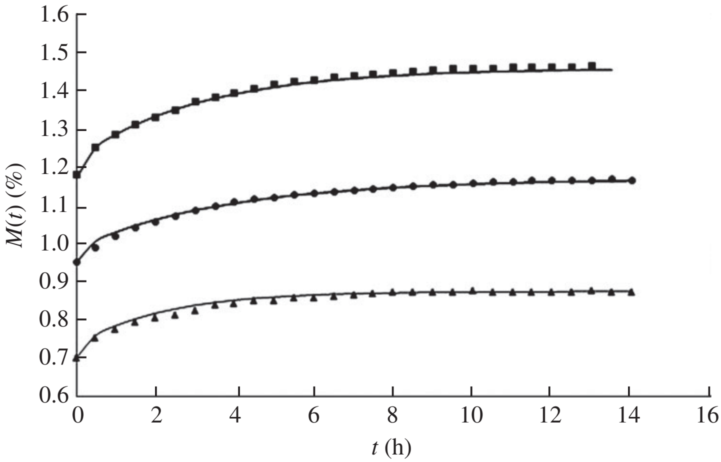

Figure 8. Moisture uptake of *urushi* samples as a result of a step change in relative humidity from 30 to 40% (triangles), 40 to 50% (circles) and 50 to 60% (squares).

Table 4. Average values of diffusion coefficient under different relative humidities.

RH	40%	50%	60%
D (m^2s^{-1})	2.26×10^{-13}	1.78×10^{-13}	2.02×10^{-13}

Equation (3.11) can be integrated with respect to x to determine the total mass of the diffusing substance at any time, $M(t)$:

$$M(t) = M(\infty) + \frac{8(C_0 - C_s)t_f A}{\pi^2} \sum_{j=0}^{\infty} \frac{1}{(2j+1)^2} \exp\left(-\left(\frac{(2j+1)\pi}{t_f}\right)^2 Dt\right), \quad (3.12)$$

where $M(\infty)$ is the mass at saturation. Equation (3.12) was used to perform a curve fitting to the experimental data (averaged moisture uptake data from experimental results of three samples for each absorption condition) shown in figure 8. A satisfactory agreement was found and D for different RHs is shown in table 4.

The absorption isotherm of water was modelled using the Guggenheim–Anderson–de Boer (GAB) equation:

$$M(\infty) = \frac{M_m A C a_w}{(1 - A a_w)(1 - A a_w + A C a_w)}, \quad (3.13)$$

where a_w is water activity, which is equal to RH/100, M_m is the monolayer moisture content, and A and C are constants related to heat of sorption (Timmermann *et al.* 2001). Figure 9 shows a good fit of equation (3.13) to the experimental data, with the fitted equation constants given in table 5.

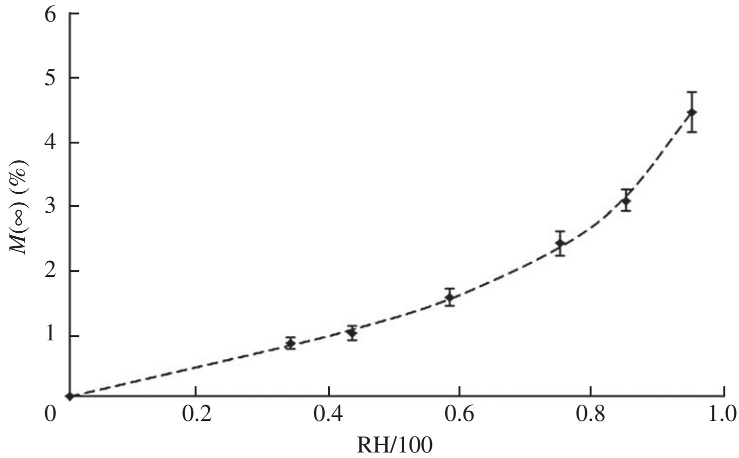

Figure 9. Equilibrium weight gain, $M(\infty)$, as a function of relative humidity. The dashed line (GAB fit) represents a fit of equation (3.12) to the experimental results (diamonds), with error bars showing s.d.

Table 5. Parameters of GAB function for modelling relationship between equilibrium weight gain ($M(\infty)$) and relative humidity for *urushi* films.

M_{m} ((kg water)/(kg dry basis))	A	C
0.0113	0.811	2.84

4. Model solution and results

A finite element model of Elmahdy's experiments (Elmahdy *et al.* 2011) was created using the commercial FE package ABAQUS (v. 6.9 and 6.10; Dassault Systems, Providence, RI, USA). The solution domain is shown in figure 10. The axisymmetry of the problem enabled simplification of the disc system used in the experiments by applying axisymmetric boundary conditions along the central axis of the disc and modelling the slice of the disc illustrated in figure 10 using two-dimensional axisymmetric elements. As seen in the figure, the disc is supported at its outer edge in the y-direction but allowed to translate freely in the x-direction. The mesh consisted of 17052, eight-node quadrilateral, elements, as illustrated in figure 11. A semi-coupled hygro-mechanical analysis was performed using the ABAQUS Standard solver in which hygroscopic strains from a transient diffusion analysis were passed to the mechanical analysis at an incremental level.

In order to develop a multi-dimensional material model, the rheological model described by equation (3.1) was extended to multidimensional stress space. In this case, the multi-direction creep strain rate, $\dot{\varepsilon}^{\mathrm{c}}_{ij}$, was determined using an associated flow law (Dunne & Petrinic 2005):

$$\dot{\varepsilon}^{\mathrm{c}}_{ij} = \dot{\varepsilon}^{\mathrm{c}}_{\mathrm{eq}} \frac{\partial g}{\partial \sigma_{ij}}, \tag{4.1}$$

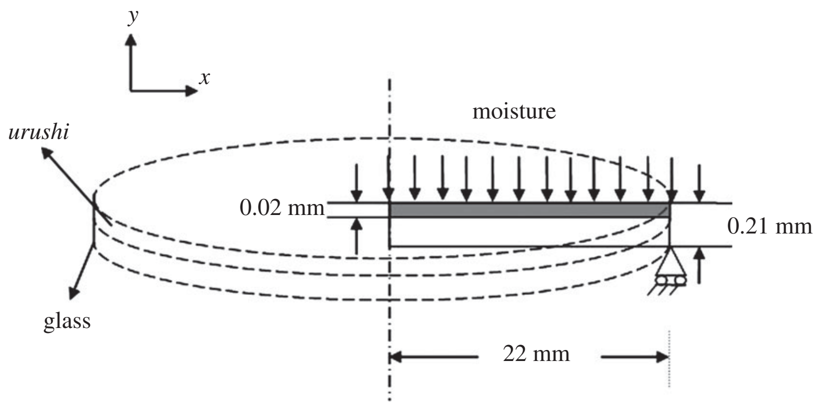

Figure 10. Simplified geometry and boundary conditions for the bi-material film samples.

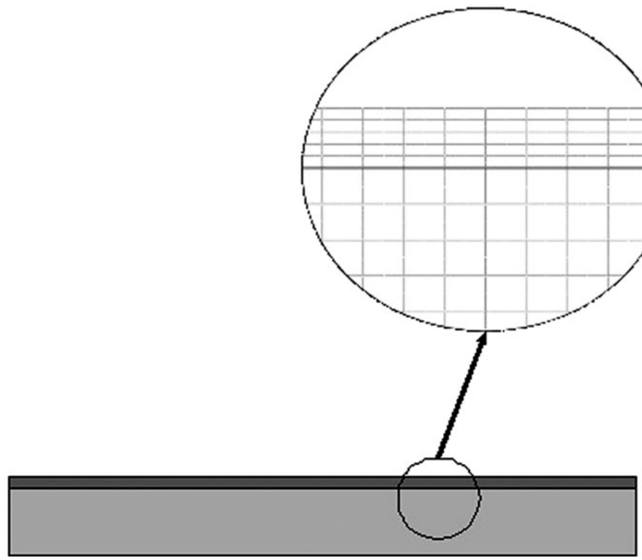

Figure 11. Detail of finite element mesh for the axisymmetric bi-layer domain.

where $\dot{\varepsilon}^{\mathrm{c}}_{\mathrm{eq}}$ is a scalar value representing an equivalent creep strain rate, g is the flow potential that can be related to an equivalent stress function and i and j represent directions of the stress tensor. The equivalent creep strain rate at any time can then be calculated through a creep constitutive equation, the parameters of which can be determined through curve fitting to uniaxial creep tensile test data (§3*a*). In this case, a flow law based on the von Mises equivalent stress was used, and equation (4.1) can then be written as

$$\dot{\varepsilon}^{\mathrm{c}}_{ij} = \frac{3}{2}\dot{\varepsilon}^{\mathrm{c}}_{\mathrm{eq}}\frac{S_{ij}}{\sigma_{\mathrm{eq}}}. \tag{4.2}$$

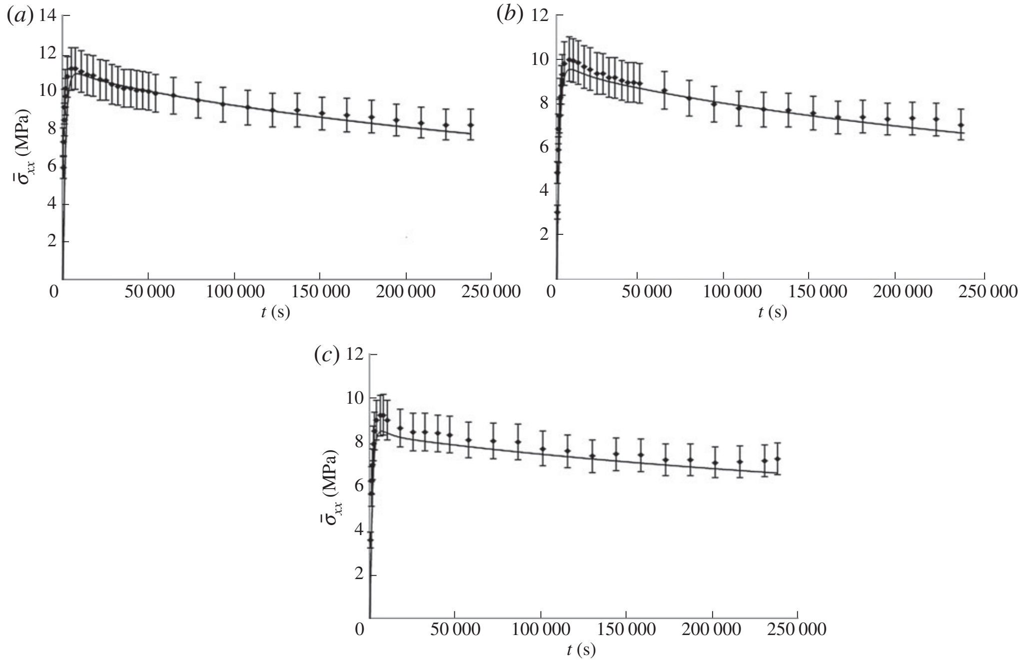

Figure 12. (*a*) Comparison of experimental (symbols) and predicted (solid line) depth averaged stress as a function of conditioning time when a bi-material sample saturated under 75% RH was placed into a chamber with humidity of 30% RH. (*b*) Comparison of experimental (symbols) and predicted (solid line) depth averaged stress as a function of conditioning time when a bimaterial sample saturated under 75% RH was placed into a chamber with humidity of 36% RH. (*c*) Comparison of experimental (symbols) and predicted (solid line) depth averaged stress as a function of conditioning time when a bi-material sample saturated under 75% RH was placed into a chamber with humidity of 42% RH.

where S_{ij} is the deviatoric stress tensor and $\boldsymbol{\sigma}_{\mathrm{eq}}$ is the von Mises equivalent stress. This model was implemented in ABAQUS using a user-defined material model encoding equation (3.1). Recovery was neglected in this analysis, because for most in service conditions there is likely to be a positive stress leading to creep dominating the response.

The boundary conditions in the bi-material disc model were such that the lower edge of the disc was only free to displace in a direction that was perpendicular to the disc's axis of symmetry. The moisture boundary conditions were a constant moisture content at the upper surface determined using equation (3.13) for the set environmental RH and zero flux at the interface between the lacquer and the substrate. Initially, the right-hand boundary was allowed to be permeable under the same conditions as the upper surface, but the depth-to-breadth ration was found to be sufficiently small that radial fluxes were insignificant and as a consequence, all the numerical experiments discussed in this study were performed with an impermeable sidewall. The values of the material properties were all specified from the experimentally determined parameters discussed in §3 of this study, and the boundary conditions were specified to replicate the experimental conditions for the bi-layer disc.

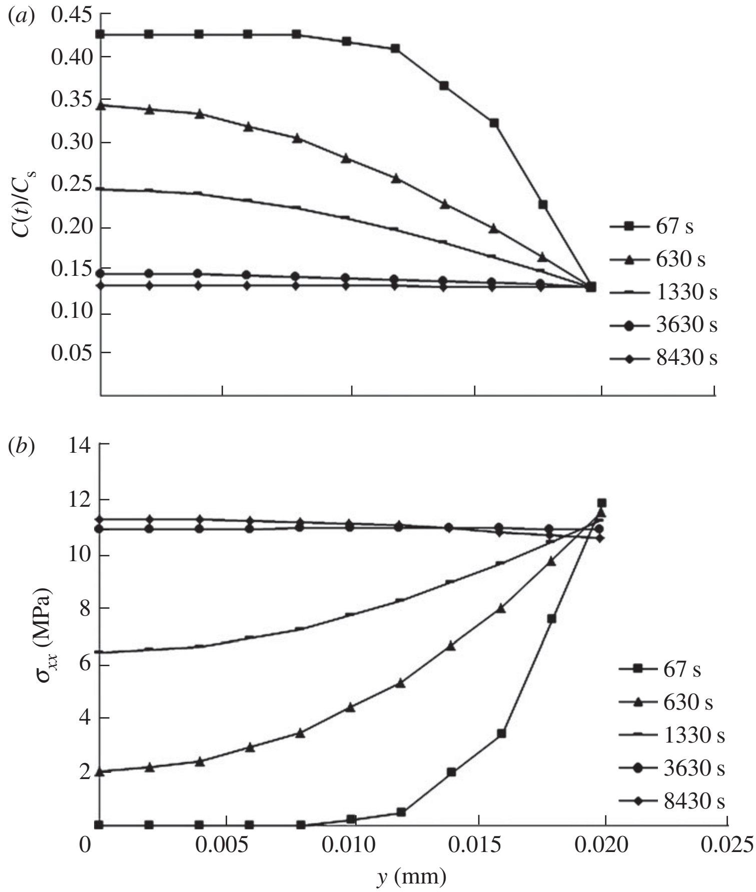

Figure 13. (*a*) Distribution of normalized moisture concentration, C, as a function of depth, y, where $y = 0$ is the *urushi*-substrate interface and the *urushi* upper surface is at $y = 0.02$, using the boundary conditions shown in figure 10 and a moisture variation from 75% to 30% RH. (*b*) Distribution of longitudinal stress, (σ_{xx}), as a function of depth, y, where $y = 0$ is the *urushi* substrate interface and the *urushi* upper surface is at $y = 0.02$, using the boundary conditions shown in figure 10 and a moisture variation from 75% to 30% RH.

Figure 12*a–c* shows the variation in the depth-averaged longitudinal stress, $\bar{\sigma}_{xx}$, with time for the bi-material samples exposed to three different conditions: changing the RH from 75 per cent RH to 30 per cent RH, 36 per cent RH and 42 per cent RH, respectively. The plotted points indicate the experimental results, and the error bars show the standard error in the measurement. The initial behaviour of the *urushi* film following a reduction in humidity is a hygroscopic shrinkage, which is constrained by the substrate, resulting in a tensile in-plane stress developing in the film. It can be seen from figure 12*a* that the stress increases rapidly in the first few minutes, reaching a maximum value of approximately 11 MPa after approximately 8000 s. After this time, there is a gradual reduction in the stress. A second effect of the desorption of the moisture is that the viscoelastic properties of the *urushi* film change, as discussed in §3*a*, and this effect was also included in the model by having moisture-dependent

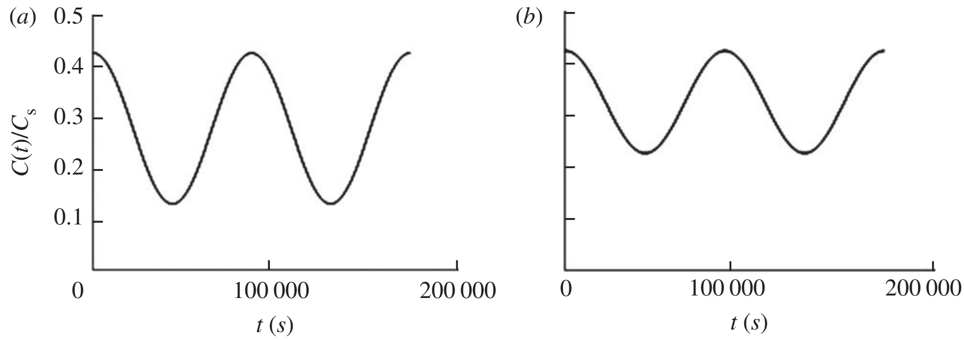

Figure 14. (*a*) Changes of normalized moisture content of *urushi* film at surface when a sample experiences a sinusoidally varying humidity during 48 hours, with a peak to peak RH of 75 to 30%. (*b*) Changes of normalized moisture content of *urushi* film at surface when a sample experiences a sinusoidally varying humidity during 48 hours, with a peak to peak RH of 75 to 50%.

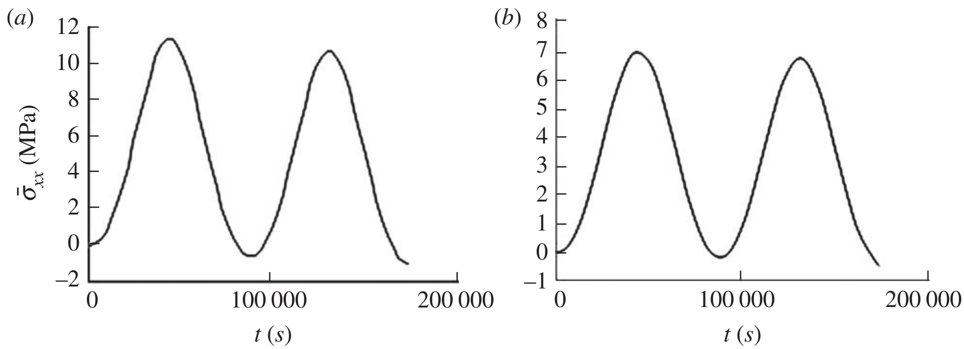

Figure 15. (*a*) Depth-averaged stress evolution of *urushi* film when a bi-material sample saturated under 75% RH experiences a sinusoidally varying humidity during 48 hours, with a peak to peak RH of 75 to 30%. (*b*) Depth-averaged stress evolution of *urushi* film when a bi-material sample saturated under 75% RH experiences a sinusoidally varying humidity during 48 hours, with a peak to peak RH of 75 to 50%.

properties in the mechanical analysis. Following the initial increase in film stress, there is a gradual reduction of the stress, which can be attributed to the relaxation of the material that arises as a result of its viscoelastic nature. The solid lines in figure 12 indicate the results from the semi-coupled hygro-stress model with the measured constitutive parameters discussed in §3. It can be seen that there is a close correspondence between the model predictions and the experimental results, with the model results lying within the bounds of the experimental error at all times. In particular, it can be seen that the model captures the rapid increase in depth-averaged stress during the early ingress phase, and accurately predicts the relaxation of the material at longer times. The good agreement between model and experiment suggests that the proposed hygro-mechanical model and the viscoelastic constitutive model provide a good phenomenological description of the observed behaviour, presenting a platform on which descriptions of models for the conservation of *urushi* can be built.

Having validated the method, it is interesting to examine the development of stresses as a function of depth. In figure 13*a*, the evolution of the moisture concentration through the *urushi* film thickness over time after the RH is reduced from 75 to 30 per cent is shown. It can be seen that shortly after the change in RH, e.g. at 67 s, the change in moisture concentration is localized to the region near to the upper surface and the moisture concentration gradient near to the substrate is zero, suggesting that a gradient in stress should be expected. Indeed, from the calculated stresses at the corresponding times, as shown in figure 13*b*, it can be seen that at short times the hygroscopic stresses are limited to the area near to the surface. As the experiment proceeds, the moisture concentration gradient reduces and as the moisture approaches a constant as a function of depth an almost uniform longitudinal stress is reached, although it is noted that the peak stress is largest at short times.

The model also allows the effects of a slowly cycling moisture content to be predicted, which is likely to be of interest because this is often the case for museum-stored artefacts. Figure 14 shows a time-dependent RH profile that varies between 70 and 30 per cent RH and between 70 and 50 per cent RH with a period of 48 h. The model predicts a time-dependent, depth-averaged stress profile that oscillates in phase with the moisture variation, but with a decaying envelope attributable to the viscoelasticity, as shown in figure 15. Interestingly, periods of compression can be seen after the first cycle that may cause in-film buckling after delamination. This indicates that further work should be carried out on the response of the material to transient loads and on the modes of failure in the material.

5. Summary and conclusions

A hygro-mechanical FE model of *urushi* behaviour based on a moisture-dependent viscoelastic phenomenology has been developed and tested. Through careful determination of the mechanical behaviour, the constitutive properties of a thin layer of lacquer were determined and used as an input to a FE-based model of the deformation and stresses that develop in response to changes in the environmental conditions. The model was validated using experimental results that show the depth-averaged stress in a thin layer of *urushi* deposited on a glass substrate. The model was used to gain insights into the time-dependent and spatially varying stresses within the layer. These showed that the regions of highest stress were to found in areas of highest moisture ingress, emphasizing the need to control the environment in which *urushi*-coated artefacts are stored. Japanese lacquer, however, is usually made up from multiple layers of *urushi* and clay, which are then deposited on a wooden substrate, which is also sensitive to humidity change. Therefore, in future, a more complex model than the current analysis is needed to represent the behaviour of a full lay-up of *urushi*.

References

Atkinson, A. 1997 Generation and relief of stress in ceramic films. *Br. Ceramic Proc.* **54**, 1–14.

Bratasz, L., Kozlowski, R., Kozlowska, A. & Rivers, S. 2008 Conservation of the Mazarin Chest: structural response of Japanese lacquer to variations in relative humidity. In *ICOM-CC triennial meeting*, vol. II, pp. 933–940. New Delhi, India.

Crank, J. 1975 *The mathematics of diffusion*. Oxford, UK: Clarendon Press.

Dunne, F. & Petrinic, N. 2005 *Introduction to computational plasticity*. Oxford, UK: Oxford University Press.

Elmahdy, A. E., Ruiz, P. D., Wildman, R. D., Huntley, J. M. & Rivers, S. 2011 Stress measurement in East Asian lacquer thin films owing to changes in relative humidity using phase-shifting interferometry. *Proc. R. Soc. A* **467**, 1329–1347. (doi:10.1098/rspa.2010.0414)

Lagarias, J. C., Reeds, J. A., Wright, M. H. & Wright, P. E. 1998 Convergence properties of the nelder: mead simplex method in low dimensions. *SIAM J. Optimization* **9**, 112–147. (doi:10.1137/S1052623496303470)

Liu, X., Elmahdy, A. E., Ashcroft, I. A. & Wildman, R. D. 2010 East Asia Lacquer: material culture, science and conservation. In *A methodology for modelling the mechanical response of urushi lacquer under varying environmental conditions* (eds S. Rivers, R. Faulkner & B. Pretzel), pp. 83–91. London, UK: Archetype Publications.

Liu, X., Elmahdy, A. E., Wildman, R. D., Ashcroft, I. A. & Ruiz, P. D. 2011 Experimental investigation and material modelling of fresh and UV aged Japanese lacquer (*urushi*). *Prog. Org. Coatings* **70**, 160–169. (doi:10.1016/j.porgcoat.2010.09.020)

Liu, X., Wildman, R. D. & Ashcroft, I. A. 2012 Experimental investigation and numerical modelling of the effect of the environment on the mechanical properties of polyurethance lacquer films. *J. Mater. Sci.* **47**, 5222–5231. (doi:10.1007/s10853-012-6406-2)

McSharry, C., Faulkner, R., Rivrers, S., Shaffer, M. S. P. & Welton, T. 2007 *The chemistry of East Asian lacquer: a review of the scientific literature*. London, UK: ROYAUME-UNI: International Institute for Conservation of Historic and Artistic Works.

Morita, Y., Arakawa, K. & Todo, M. 2008 Experimental analysis of thermal displacement and strain distributions in a small outline J-leaded electronic package by using wedged-glass phase-shifting moiré interferometry. *Opt. Lasers Eng.* **46**, 18–26. (doi:10.1016/j.optlaseng.2007.08.007)

Obataya, E., Ohno, Y., Norimoto, M. & Tomita, B. 2001 Effects of oriental lacquer(*urushi*) coating on the vibrational properties of wood used for the soundboards of musical instruments. *Acoust. Sci. Technol.* **22**, 27–34. (doi:10.1250/ast.22.27)

Obataya, E., Furuta, Y., Ohno, Y., Norimoto, M. & Tomita, B. 2002 Effects of aging and moisture on the dynamic viscoelastic properties of oriental lacquer (*urushi*) film. *J. Appl. Polym. Sci.* **83**, 2288–2294. (doi:10.1002/app.2321)

Ogawa, T. & Kamei, T. 2000 The fracture of lacquer films on oriental Lacquerware resulting from absorption and desorption of water. In *Japanese and European Lacquerware*, vol. 96, pp. 160–169. Munich, Germany: Arbeitshefte des Bayerischen Landesamtes fur Denkmalpflege.

Ogawa, T., Inoue, A. & Osawa, S. 1998*a* Effect of water on viscoelastic properties of oriental lacquer film. *J. Appl. Polym. Sci.* **69**, 315–321. (doi:10.1002/(SICI)1097-4628(19980711)69:2<315::AID-APP12>3.0.CO;2-V)

Ogawa, T., Arai, K. & Osawa, S. 1998*b* Light stability of oriental lacquer films irradiated by a fluorescent lamp. *J. Polym. Environ.* **6**, 59–65. (doi:10.1023/A:1022830629581)

Rivers, S. 2003 On the conservation of the Mazarin Chest. In *27th Int. Symp. Conservation and Restoration of Cultural Property*, pp. 150–158. Tokyo, Japan: Tokyo National Research Institute for Cultural Property/Tokyo National Museum.

Ruiz, P. D., Jumbo, F. S., Seaton, A., Huntley, J. M., Ashcroft, I. A. & Swallowe, G. M. 2006 Numerical and experimental investigation of three-dimensional strains in adhesively bonded joints. *J. Strain Anal. Eng. Design* **41**, 583–596. (doi:10.1243/03093247JSA180)

Saleem, Q., Wildman, R. D., Huntley, J. M. & Whitworth, M. B. 2003 A novel application of speckle interferometry for the measurement of strain distributions in semi-sweet biscuits.*Meas. Sci. Technol.* **14**, 2027–2033. (doi:10.1088/0957-0233/14/12/001)

Saleem, Q., Wildman, R. D., Huntley, J. M. & Whitworth, M. B. 2005 Improved understanding of biscuit checking using speckle interferometry and finite-element modelling techniques. *Proc. R. Soc. A* **461**, 2135–2154. (doi:10.1098/rspa.2005.1469)

Stoney, G. 1909 The tension of metallic films deposited by electrolysis. *Proc. R. Soc. A* **82**, 172–175. (doi:10.1098/rspa.1909.0021)

Taguchi, K., Hirose, S. & Abe, Y. 2007 Photo-curing composite paint containing urushi (Oriental lacquer), and wrinkled coating caused by phase separation. *Prog. Org. Coatings* **58**, 290–295. (doi:10.1016/j.porgcoat.2007.01.001)

Timmermann, E. O., Chirife, J. & Iglesias, H. A. 2001 Water sorption isotherms of foods and foodstuffs: BET or GAB parameters? *J. Food Eng.* **48**, 19–31. (doi:10.1016/S0260-8774(00)00139-4)

Yang, L., Zhang, P., Liu, S., Samala, P. R., Su, M. & Yokota, H. 2007 Measurement of strain distributions in mouse femora with 3D-digital speckle pattern interferometry. *Opt. Lasers Eng.* **45**, 843–851. (doi:10.1016/j.optlaseng.2007.02.004)

Zhang, J., Jiang, D., Tan, S., Gui, L. & Ruan, H. 2002 Aqueous processing of SiC green sheets. II. Binder and plasticizer. *J. Mater. Res.* **17**, 2019–2025. (doi:10.1557/JMR.2002.0299)